Pergamon

Cement and Concrete Research, Vol. 28, No. 3, pp. 381–390, 1998

0008-8846/98 $19.00 + .00

PII S0008-8846(98)00007-6

THERMAL DECOMPOSITION OF HYDRATED ALUMINA CEMENT (CAH_{10})

F. Guirado,[1]* S. Galí,* and J.S. Chinchón†
*Dep. Cristal·lografia i Mineralogia, Universitat de Barcelona, C/Martí i Franquès s/n, 08028 Barcelona, Spain
†Dep. Construccions Arquitectòniques, Universitat d'Alacant, Ap. Correus 99, 03080 Alacant, Spain

(Received January 14, 1997; in final form January 14, 1998)

ABSTRACT

It is known that the initial product of hydration of high-alumina cement at low temperatures, often labeled "CAH_{10}," contains both crystalline and amorphous portions. The thermal decomposition of this product was studied in several samples. This study was carried out by two different methods: derivative thermogravimetric analysis (DTG) and x-ray diffraction (XRD) combined with temperature. The DTG signal of the compound was decomposed in four different kinetic processes. The nature of the water liberated in each process was characterized by the shape parameters of the process. The x-ray diffractograms at different temperatures showed two volume variations of the CAH_x compound, related to contractions in the c parameter before the collapse of the structure to yield an amorphous phase. Two of the four observed processes are related to the dehydration of the crystalline portion and the other two to the amorphous dehydration.

Introduction

The hydration of CA yields a complex product, still not well characterized. There are several unknowns that can be approximated through thermogravimetric analysis. One is the initial amount of amorphous phase (gel), that seems to depend on the temperature of hydration (1), and slowly crystallizes with time (2,3). The water content of the crystalline portion may depend on the relative humidity (4), whereas the hydration degree of the amorphous portion is unknown. Classically, the gel has been considered an alumina gel (5,6,7), but other authors have observed varying amounts of calcium (8), even with a C/A ratio close to unity (9,10). Several authors proposed the hypothesis that the gel is a precursor of the crystalline phase (11). Taking into account all these considerations, we propose that the hydration of CA takes place according to the following reaction ($<20°C$):

[1]Address correspondence to F. Guirado at his present address: Servei di Recursos Cientifics, Universitat Roviral i Virgili, Tarragona, Spain.

$$CA + H\ (\text{excess}) \rightarrow a{\cdot}CAH_x\ (\text{cryst.}) + (1 - a){\cdot}CAH_y\ (\text{gel})$$

$$(x \approx 6,\ y \text{ variable},\ 0 \leq a \leq 1)$$

At room temperature, the CAH_{10} slowly (over several years) transforms to the so-called "cubic" phase, and gibbsite, according to the following reaction:

$$3{\cdot}CAH_{10} \rightarrow C_3AH_6 + 2{\cdot}AH_3 + H$$

cubic phase gibbsite

The structural properties of aluminous cement are affected by the previous transformation. The study of the differential thermal analysis (DTA) and derivative thermogravimetric analysis (DTG) curves of the hydrated aluminous cement have been used to measure its transformation (12). The DTG curve is more advantageous than the DTA because it has a straight base line that permits quantification of the process that takes place. Moreover, the DTG curves have marked inflexion points and plateaux, features that are not present in the TG measured curves.

However, the overlapping of the different processes on the DTG curve is very important. Between the two main peaks of a DTG curve a plateau can be observed far from the base line. Because the baseline in DTG curves is a straight line at $dw/dt = 0$, the plateau indicates that there is a considerable rate of weight change between these peaks (13).

In this work, we have studied the thermal decomposition of the so-called CAH_{10} by means of the DTG curve decomposition on the basis of different kinetic processes. The kind of water liberated in each process has been characterized. DTG results were correlated with those obtained by XRD.

Theoretical Considerations

The rate of a non-isothermal reaction, like that taking place in thermogravimetry, can be expressed as

$$\frac{d\alpha}{dt} = g(T)\, f(\alpha) \tag{1}$$

where α is the conversion degree, $f(\alpha)$ is a function that represents the hypothetic model that controls the reaction mechanism, and $g(T)$ is a rate constant that depends on the temperature. The function $g(T)$ is assumed to take the Arrhenius form:

$$g(T) = A\, e^{-\frac{E}{RT}} \tag{2}$$

where A is the preexponential factor, E the activation energy, and R the universal gas constant. The conversion degree is expressed by:

$$\alpha = \frac{P_t}{P_\infty} \tag{3}$$

where P_t and P_∞ denote the weight lost at instant t and at the end of the process, respectively.

If we suppose a constant heating rate $\beta = dT/dt$, then Eq. 1 can be expressed as:

$$\frac{d\alpha}{dT} = \left(\frac{A}{\beta}\right) e^{-\frac{E}{RT}} f(\alpha) \tag{4}$$

Integrating the last expression we obtain:

$$\int_0^1 \frac{d\alpha}{f(\alpha)} = \int_{T_1}^{T_2} \left(\frac{A}{\beta}\right) e^{-\frac{E}{RT}} dT = \frac{EA}{R\beta} p(x) \tag{5}$$

where $p(x)$ is the truncated expansion of Schlomilch (14), expressed by:

$$p(x) = e^{-x} \left(\frac{1}{x}\right) \left(\frac{1}{x+2}\right) \qquad x = \frac{E}{RT} \tag{6}$$

The elucidation of the mechanisms of a reaction from TG data is not a well-resolved problem (15,16). Several authors have been using different mathematical methods in order to determine the mechanism that governs a given reaction (17–21).

DTG curve better marks all different processes that take place in any thermal decomposition than its primitive precursor, TG. A change in TG slope is reflected as a marked peak in DTG. In this sense, any process can be represented, theoretically, as a peak function. By analyzing the peak it is possible to obtain several parameters as the temperature at different decomposition degrees, the mass loss in each process and the kinetic parameters described previously.

Several kinetic models were proposed to describe the different thermal processes observed through DTG and DTA (22,23). Among them, Coats-Redfern model (18) and the so-called Avrami equation (24,25) were selected, because they fitted more acurately our experimental data. In the first model $f(\alpha) = (1\text{-}\alpha)^n$, n being the order of reaction, and in the second $f(\alpha) = 2(1 - \alpha)[-\ln(1 - \alpha)]^{1/2}$.

Experimental

The CA phase was obtained by heating at 1300°C for 200 h an equimolar mixture of pure reactants Al_2O_3 and $CaCO_3$ (Merck purity). The reaction advance was controlled by XRD periodically. The final sintered compound was finely milled and sieved below $<10\mu$. The hydration of CA was carried out at 5°C in excess water, and periodic stirring. Final product was filtered, washed with acetone and characterized by x-ray diffraction. To compare these laboratory samples with commercial cement, samples of a Spanish aluminous cement "Electroland" were hydrated with different proportions w/c (water/cement) and cured for 28 days at room temperature. The commercial samples were hydrated under stanadard conditions used in cement laboratories. Laboratory samples were prepared in order to obtain a complete hydration of CA phase by changing w/c ratio, hydration time, and stirring period. Table 1 shows the hydration conditions for the laboratory and commercial samples, numbered from 1 to 7.

Thermogravimetric analysis for samples 1 to 6 were performed with a SETARAM TG DTA92 at different heating rates (1 and 5°/min.) from 20 to 300°C in Ar at 2l/h as atmosphere. Sample 7 was analyzed with a NETZSCH STA 409 C in N_2 flux at 1l/h as atmosphere.

X-ray diffraction analyses with temperature (XRDT) were performed with a SIEMENS-D500 diffractometer equiped with a positional sensitive detector (PSD). The experimental

TABLE 1
Hydration conditions and experimental conditions of TG and XRDT analyses for the samples studied.

Sample	Initial Comp.	w/c	Phases[1]	T(°C)	t	Analysis	β	mg.	Range (°C)	Analysis label
1	CA	50	CAH_{10}	5°	7 days	TG	1	138	20-300	TG1-1
							5	155	20-300	TG1-5
2	Electroland[3]	0.3	CAH_{10}+CA[2]	20°	28 days	TG	5	431	20-500	TG2-5
3	Electroland[3]	0.25	CAH_{10}+CA[2]	20°	28 days	TG	5	453	20-500	TG3-5
4	Electroland[3]	0.2	CAH_{10}+CA[2]	20°	28 days	TG	5	570	20-500	TG4-5
5	CA	200	CAH_{10}	5°	13 days	TG	1	153	20-300	TG5-1
						XRDT	1	-	20-300	XRDT
6	CA	80	CAH_{10}	5°	46 days	TG	1	134	20-300	TG6-1
7	CA	48	CAH_{10}	5°	9 days	TG	1	77	20-600	TG7-1
							5	79	20-600	TG7-5

[1] Detected by XRD
[2] and other minor phases.
[3] Chemical composition in weight per cent of oxides determined by x-ray fluorescence was: 39.3 Al_2O_3; 38.0 CaO; 2.6 SiO_2; 1.5 TiO_2; 14.3 Fe_2O_3; 0.3 MgO.

conditions were: temperature range from 20 to 300°C, heating rate at ≈1°/min., step size of 0.05°2θ, and counting time of 6s. One scan was measured each 20°C. Cu K_α radiation was used. Table 1 shows the different analyses done for each sample.

Results

TG

A simple view of a DTG curve suggests that the whole curve is a sum of two different processes, marked by two main peaks (Fig. 1). By comparing sample 1 analyzed at 1 and 5°/min, one can observe a small shoulder on the low temperature side of the first peak, which corresponds to a process that is partially overlapped. This small peak can only be observed clearly at low heating rates because at higher rates it is completely overlapped. Between two main peaks, instead of a valley there is a pronounced plateau due to a fourth process. In summary, we assume that the water of CAH_{10} is lost in four different processes.

The decomposition of each DTG curve was done by using a program that fit the observed data to the sum of four given kinetics models. This program works inside the MATHEMATICA environment (Wolfram Research, Inc.). We followed two criteria to assign a model (Coats-Redfern or Avrami equation) to each process: the similitude of preexponential factors at different heating rates (β) for the same sample; and, on the other hand, the model combination that gave us the minimum error *R*, according to the expression:

$$R = \frac{\Sigma\,[Obs_t - Calc_i]^2}{\Sigma\,[Obs_i]^2} \qquad (7)$$

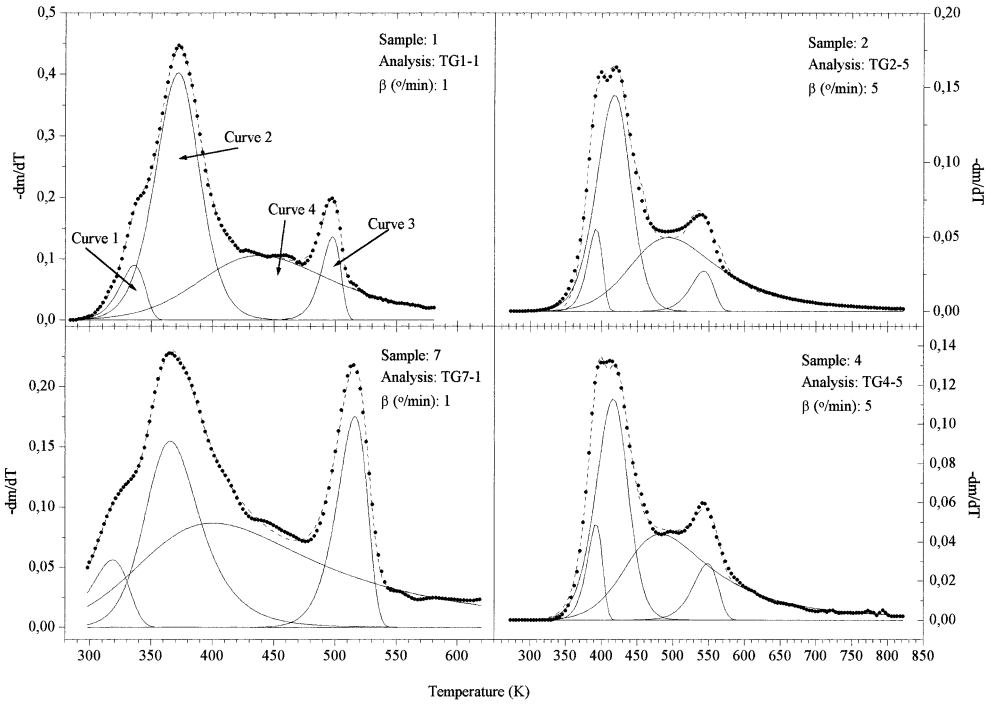

FIG. 1.
Experimental DTG data (*dots*), calculated DTG (*dashed line*), and calculated individual processes (*solid line*) for samples 1, 2, 4, and 7.

Figure 1 shows the DTG curve observed and decomposed as a sum of four processes for TG1–1, TG2–5, TG4–5, and TG7–1 analysis. The best fittings were obtained by decomposing the curves of TG1–1 and TG1–5 in four curves as follows: Coats-Redfern model for curves 2nd and 4th (with $1 \leq n \leq 6$), and two-dimensional growth model for curves 1st and 3rd. All samples were fitted according to this scheme.

The slope of DTA peaks is currently described by several shape factors that are related to the activation energy, the preexponential factor, and the order of the reaction (*E*, *A*, and *n* respectivelly). Both shape factors and kinetic parameters were used to characterize the water released by different processes and to identify the reaction type (26). We have calculated the following shape parameters of asymmetry and width (27) for each calculated curve of the DTG analysis:

$$\Delta T(0.8;0.2) = T_{0.8} - T_{0.2} \qquad \% = \alpha_{T(max)}$$

$$T_1/T_2 = \frac{area_{T(0.2;max)}}{area_{T(max;0.8)}} \qquad R_{max} = \frac{\Delta T(T_{max};T_{0.2})}{\Delta T(T_{0.8};T_{0.2})} \tag{8}$$

The peak width is estimated by $\Delta T(0.8;0.2)$, which is the difference of temperatures for 20 and 80% of conversion degree ($T_{0.2}$ and $T_{0.8}$). Peak asymmetry is evaluated by the following factors: %, which gives the degree of conversion at the maximum rate of decomposition; T_{max}; T_1/T_2, the ratio between the peak area before and after T_{max}; and R_{max}, the ratio between

TABLE 2
Total weight loss (%), obtained temperatures (K), shape factors, and residuals from DTG curve analyses for the studied samples.

Analysis	Peak	T(max)	T(0.2)	T(0.8)	%	T_1/T_2	R(max)	R
TG1-1	1	336	322	341	61.2	1.57	0.72	
total weight loss	2	372	355	387	51.4	1.05	0.53	
37.7%	3	498	487	502	62.1	1.64	0.74	
	4	438	406	522	39.3	0.65	0.28	1.92
TG1-5	1	394	372	402	60.6	1.53	0.71	
	2	424	403	439	55.7	1.22	0.60	
37.56%	3	540	527	546	62.1	1.63	0.74	
	4	488	460	589	36.7	0.59	0.22	2.03
TG2-5	1	389	373	394	61.4	1.58	0.72	
	2	416	405	463	37.0	0.55	0.20	
19.29%	3	526	487	544	59.2	1.44	0.68	
	4	544	545	700	19.4	0.26	0.01	1.96
TG3-5	1	391	375	397	61.3	1.57	0.72	
	2	416	412	482	25.3	0.34	0.05	
18.45%	3	542	516	553	61.0	1.55	0.71	
	4	547	449	627	38.3	0.63	0.25	2.72
TG4-5	1	389	374	395	61.4	1.58	0.72	
	2	415	404	462	34.2	0.52	0.18	
15.63%	3	548	524	558	61.1	1.56	0.72	
	4	527	505	652	33.7	0.51	0.15	2.00
TG5-1	1	337	323	343	61.0	1.56	0.72	
	2	366	355	390	40.9	0.69	0.31	
42.06%	3	485	476	489	62.3	1.65	0.74	
	4	443	417	518	38.5	0.62	0.26	2.95
TG6-1	1	344	329	350	61.0	1.56	0.72	
	2	377	360	384	60.5	1.53	0.71	
40.57%	3	480	449	494	59.8	1.48	0.70	
	4	392	384	566	24.9	0.36	0.04	2.20
TG7-1	1	319	299	327	60.0	1.44	0.70	
	2	365	350	394	43.1	0.76	0.35	
41.00%	3	516	499	522	61.6	1.60	0.73	
	4	400	375	610	30.1	0.47	0.11	1.23
TG7-5	1	357	330	370	59.0	1.43	0.68	
	2	411	383	424	58.3	1.40	0.67	
41.00%	3	545	529	551	61.7	1.61	0.73	
	4	427	402	596	31.4	0.49	0.13	1.94

the difference of temperatures $T_{max} - T_{0.2}$ and $T_{0.8} - T_{0.2}$. Theoretically, it has been proved that the reaction order (n) modifies the peak width whereas the asymmetry is independent of E and A terms (27). Once these factors were calculated, they were compared with those obtained from thermal analysis of well-characterized minerals containing different kinds of water (adsorption, interlayer, structural, or crystal water, etc.) as estimated by Földvári (26). Table 2 shows the total weight loss, temperature ranges, asymmetry parameters, and R values obtained for each curve.

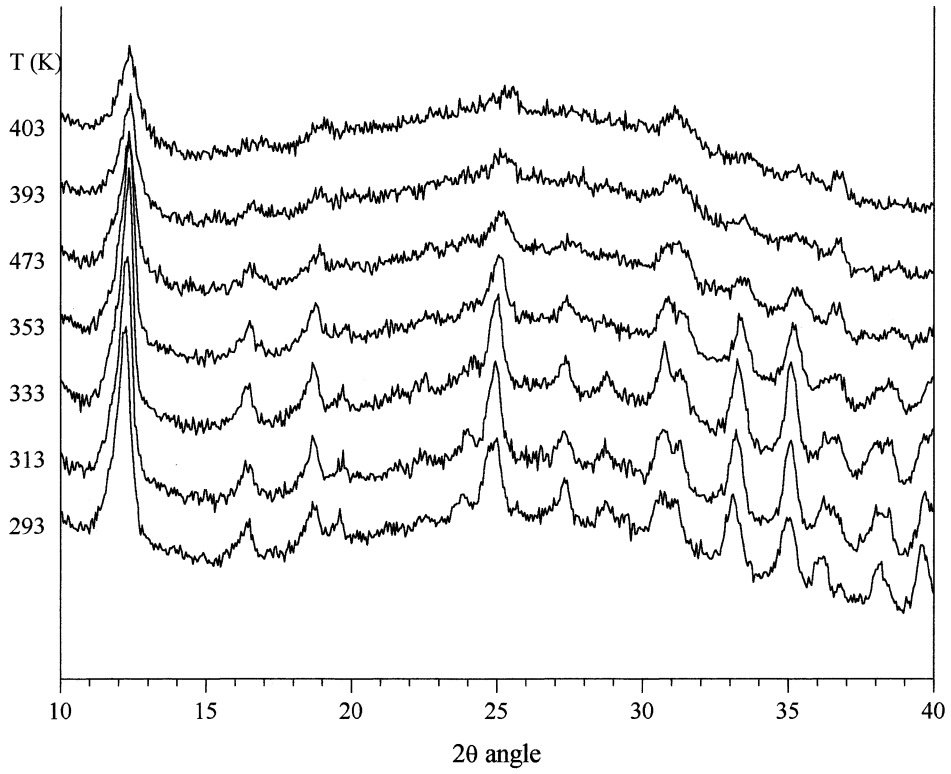

FIG. 2.
Experimental x-ray diffraction profiles obtained at diferent temperatures for sample 5. Profiles have been moved vertically. Vertical axis indicates intensity in arbitrary units.

XRDT

The cell parameters of CAH_x phase (hexagonal symmetry) were calculated for each temperature. Each XRD profile was fitted with the program FULLPROF (28) based on the Rietveld method (28). The option of this program called Pattern Matching was used, because it permits researchers to fit a XRD profile without knowing the entire crystal structure. For each XRD profile up to 420K, cell parameters, FWHM (full-width-at-half-maximum), lorentzian and gaussian contribution ([*eta*] parameter), asymmetry correction for $2\theta < 30°$ and preferred orientation (March model (30)), and intensities of all reflections were fitted. Figure 2 shows seven experimental XRD profiles obtained for sample 5 from 293 to 403K. In Figure 3, the variation of the *a*, *c*, and *V* cell parameters are depicted as a function of temperature

Discussion

The *c* lattice parameter and the volume of the cell, *V*, show two inflexions at approximately 310 K and 385 K, whereas parameter *a* shows a single inflexion at 385 K (Fig. 2). These

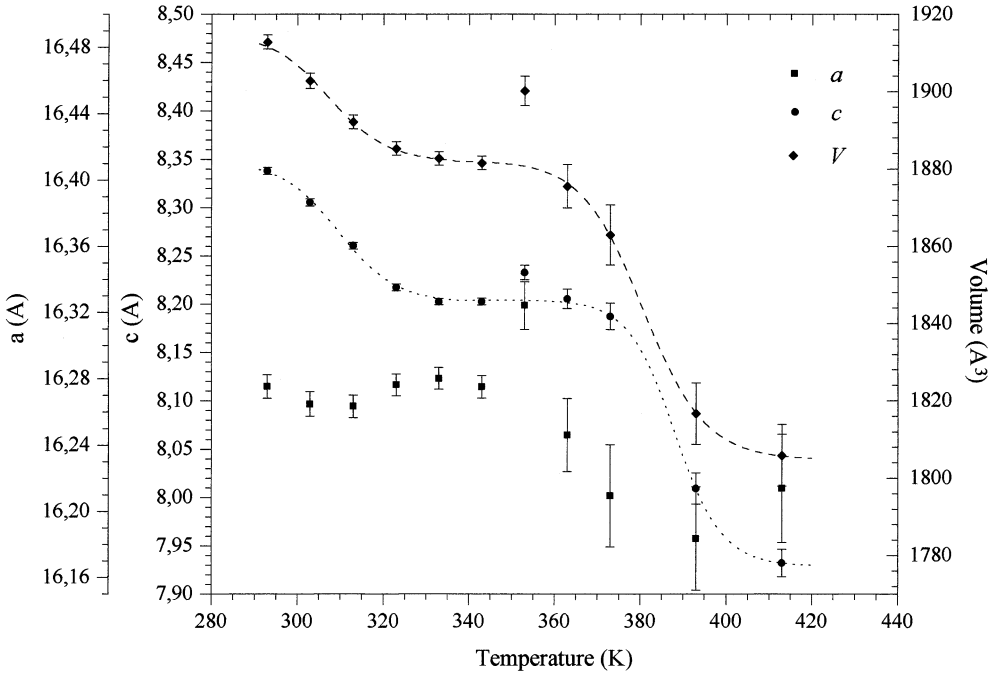

FIG. 3.
Experimental x-ray diffraction profiles obtained at different temperatures for sample 5. Profiles have been moved vertically. Vertical axis indicates intensity in arbitrary units.

inflexions take place inside or near the $T_{0.2} - T_{0.8}$ range for 1st and 2nd curves, respectively, depending on the heating rate. It is apparent that the two first curves are related to water loss of the crystalline phase CAH_x. This hypothesis is confirmed by the fact that the shape parameters for these curves are indicative of "crystalline" water, because similar shape values were obtained for different hydrated minerals (26). The first curve can be related to water located between layers normal to *c* axis, because only a reduction on *c* cell parameter was observed, whereas *a* remained constant. On the other hand, the second curve is related to structural water because there was observed a simultaneous reduction of *c* and *a* cell parameters. Once this water is released, the structure collapses. These two different roles of water molecules have been confirmed by the solution of the crystal structure from powder diffraction intensities (31).

Temperature range for the 3rd peak coincides with that of gibbsite (AH_3) decomposition described by several authors. However, no crystalline gibbsite was detected by XRD in sample 5. Because shape parameters for this 3rd peak corresponds to "crystalline" water as well, we have assumed that this gibbsite is in crypto-crystalline form, giving broad peaks with low intensity.

Shape parameters of 4th peak are indicative of "amorphous" water not attached to any crystal structure. The water lost in this process can be related to CAH_y amorphous, because no crystal changes were observed in this temperature range through thermodiffractometry. We have assigned this last curve to the decomposition of an amorphous CAH_y. In this peak, especially for commercial samples, R_{max} value is not satisfactory. The inconsistences in these

values are attributed mainly to a ill-definition of the top and tails of peak 4, which is highly correlated with all remainder peaks. It is uncertain how, for this peak, to assign a correct reaction order (n), and consequently the positions of T_{max}, $T_{0.2}$, and $T_{0.8}$ oscillate accordingly.

Conclusions

DTG curve corresponding to dehydration of CAH_{10} can be decomposed at least in four well differenced processes.

Dehydration of the crystalline portion CAH_x takes place in two steps, detected through volume variations. Water initially released at T $\approx$ 310 K is thought to be interlaminar. A subsequent more important loss of water at T $\approx$ 385 K produces the collapse of the structure.

Peak number 3 corresponds to crypto-crystalline gibbsite that can appear as a product of dehydration of amorphous CAH_y.

Peak number 4 can be related to the dehydration of the amorphous portion CAH_y.

Acknowledgments

The authors thank the Serveis Científico Tècnics de la Universitat de Barcelona for the XRD profiles and the Laboratori d'Investigació de Formacions Salines for the TGA analyses.

References

1. A. Rettel, R. Seydel, W. Gessner, J.P. Bayoux, and A. Capmas, Cem. Concr. Res. 23, 1056 (1993).
2. X. Cong and R.J. Kirkpatrick, J. Am. Ceram. Soc. 76, 409 (1993).
3. R. N. Edmonds and A.J. Majumdar, Cem. Concr. Res. 18, 311 (1988).
4. F.G. Buttler and F.W. Taylor, Il Cemento 3, 147 (1978).
5. H.G. Midgley, Trans. Brit. Ceram. Soc. 66, 161 (1967).
6. T.D. Robson, La química de los cementos, H.F.W. Taylor (ed.), Ch. 12, Urmo, Barcelona, Spain, 1967.
7. K. Fujii, W. Kondo, and H. Ueno, J. Am. Ceram. Soc. 69, 361 (1986).
8. C.S. Poons and G.W. Groves, J. Mater. Sci. Lett. 7, 243 (1988) .
9. A. Capmas, D. Menetrier-Sorrentino, and D. Damidot, Calcium Aluminate Cements, p.5, Chapman and Hall, London, 1990.
10. S.M. Bushnell-Watson and J.H. Sharp, Materiales de Construcción 42, 13 (1992).
11. B.R. Currel, R. Grzeskowlak, H.G. Midgley, and J.R. Parsonage, Cem. Concr. Res. 7, 420 (1987).
12. H.G. Midgley and A. Midgley, Mag. Concr. Res. 27, 59 (1975).
13. B. El Jazairi, Thermochim. Acta 21, 381 (1977).
14. J.H. Flynn and L.A. Wall, J. Res. Natl. Bur. Stand., Sect. A, 70, 487 (1966).
15. G.G.T. Guarini, R. Spinicci, F.M. Carlini, and D. Donati, J. Thermal Anal. 5, 307 (1973).
16. S.R. Dharwadkar, M.S. Chandrasekharaiah, and M.D. Karkhanavala, Thermochim. Acta 25, 372 (1978).
17. E.S. Freeman and B. Carrol, J. Chem. 62, 394 (1958).
18. A.W. Coats and J.P. Redfern, Nature 201, 68 (1964).
19. H.H. Horowitz and G. Metzger, Anal. Chem. 35, 1464 (1963).
20. J. Zsakó, J. Phys. Chem. 72, 2406 (1968).
21. V. Šatava and F. Škvará, J. Am. Ceram. Soc. 52, 591 (1969).
22. A. Abdu Zuru, R. Whitehead, and D.L. Griffiths, Thermochim. Acta 164, 285 (1990).

23. S. Ma, G. Huang, and J.O. Hill, Thermochim. Acta 184, 241 (1991).
24. J.H. Sharp, G.W. Brindley, and B.N. Narahari-Achar, J. Am. Ceram. Soc. 49, 379 (1966).
25. J. Sestak and B. Berggren, Thermochim. Acta 3, 1 (1971).
26. M. Földvári, Thermal Analysis in the Geosciences. W. Smykatz-Kloss, S.St.J. Warne (eds.), Lecture Notes in Earth Sciences, Vol. 38, 1991.
27. G. Pokol, S. Gáli, and E. Pungor, Thermochim. Acta 92, 82 (1985).
28. J. Rodriguez-Carvajal, Abstracts of the Satellite Meeting on Powder Diffraction of the XV Congress of the IUCr, p. 127, Toulouse, France. 1990.
29. H.M. Rietveld, J. Appl. Cryst. 2, 65 (1969).
30. W.A. Dollase, J. Appl. Cryst. 19, 267 (1986).
31. F. Guirado, S. Gáli, J.S. Chinchón, and J. Rius, Angew. Chem. Int. Ed. Engl. In press.